Journal of
Synchrotron
Radiation

ISSN 0909-0495

Received 16 December 2011
Accepted 22 February 2012

XANES analysis of spectral properties and structures of arsenate adsorption on TiO_2 surfaces

Guangzhi He, Gang Pan* and Meiyi Zhang

State Key Laboratory of Environmental Aquatic Chemistry, Research Center for Eco-Environmental Sciences, Chinese Academy of Sciences, Beijing 100085, People's Republic of China.
E-mail: gpan@rcees.ac.cn

X-ray absorption near-edge structure (XANES) of arsenate adsorption on TiO_2 surfaces was calculated using self-consistent multiple-scattering methods, allowing a structural analysis of experimental spectra. A quantitative analysis of the effect of disorder revealed that the broadening and weakening of the characteristic absorption in experimental XANES was due to the structural disorder of the arsenate–TiO_2 adsorption system. The success with calculating the scattering amplitude of a specific set of paths using the path expansion approach enables the scattering contributions of different coordination shells to the XANES to be sorted out. The results showed that the scattering resonances from high-level shells inherently overlapped onto the first-shell scattering amplitudes, and formed the fine structures in the XANES region. A variation in one oscillatory feature could be due to several structural changes affecting specific single/multiple-scattering amplitudes. Therefore, direct assignments of spectral features with structural elements should be based on adequate theoretical analysis.

Keywords: spectral analysis; adsorption; multiple-scattering method; path expansion calculation; disorder; coordination shell.

1. Introduction

X-ray absorption near-edge structure (XANES) refers to the region of the X-ray absorption spectra dominated by strong photoelectron scattering that extends 50–60 eV above an absorption edge (Ankudinov *et al.*, 1998). XANES can provide three-dimensional stereochemical information on the electronic distribution and local geometry of complex and disordered materials (Ankudinov *et al.*, 1998; Waychunas *et al.*, 2003; Zabinsky *et al.*, 1995). The sensitivity to slight geometry variations allows XANES spectra to probe the local chemical environments of low-concentration samples (Waychunas *et al.*, 2003; Khare *et al.*, 2007). Therefore, XANES is of great interest in surface science and catalysis.

XANES presents geometric and electronic information from multiple-scattering paths, while extended X-ray absorption fine structure (EXAFS) gives geometric information from single scattering (Rehr *et al.*, 1998; Waychunas *et al.*, 2003; Morin *et al.*, 2008). Therefore, XANES can provide complementary information to EXAFS measurements and lead to a more complete characterization of surface topology (He *et al.*, 2011*b*). However, compared with EXAFS, the XANES technique is of limited application owing to most XANES being typically interpreted only qualitatively, mainly *via* comparison with model compound structures (Robinet *et al.*, 2011; Nguyen *et al.*, 2011; Yan *et al.*, 2008; Huang *et al.*, 2008). Moreover, although self-consistent multiple-scattering (MS) calculations of XANES are now standard (Ankudinov *et al.*, 1998, 2002*a*; Zabinsky *et al.*, 1995), the quantitative interpretation of XANES in terms of geometrical structure has been difficult (Khare *et al.*, 2007; Moniek *et al.*, 2007). A key issue in XANES analysis is how to separate the single/multiple-scattering contributions from different coordination shells. Hence, to accurately interpret the structural origin of XANES, a way needs to be found to sort out the scattering contributions from various structural elements. Moreover, for complex and low-symmetry systems, such as ion adsorption onto mineral particles, the disorder effects are not negligible. Disorder analysis is therefore essential for direct structural comparison with experimental XANES spectra.

In an attempt to remedy these difficulties we present here a disorder-containing XANES calculation and path expansion calculation of arsenate adsorption on TiO_2 surfaces. The modeling of disorder effects on XANES fingerprinting characteristics yields an estimation of the specific disorder in samples. A clear picture of scattering amplitudes contributing to XANES from different coordination shells was obtained using the path expansion calculation.

2. Theory and experimental methods

2.1. XANES simulation

As(V) *K*-edge theoretical XANES spectra were computed using two complementary modes: the real-space full-multiple-scattering (FMS) algorithm (*i.e.* all scattering paths are summed within a specified cluster volume) and the path expansion approach (Waychunas *et al.*, 2003; Ankudinov *et al.*, 1998; Zabinsky *et al.*, 1995). The path expansion calculation with the same cluster volume as the FMS procedure was employed to evaluate the scattering contributions of different coordination shells to XANES features. The calculations by a series of Debye–Waller factors (the average of thermal and static disorder for all scattering paths over the model cluster) were carried out to estimate the disorder of the experiment system (Ankudinov *et al.*, 1998, 2002*b*) and to detect the effects of disorder on XANES. The XANES calculations were performed using a self-consistent field potential model with the *FEFF8.2* code (Ankudinov *et al.*, 2002*a*,*b*). The self-consistent field potential model is more accurate for XANES calculation than atomic overlap using the Mattheiss prescription, because the former takes the charge transfer into account and is more reliable in estimating the Fermi level E_F (Ankudinov *et al.*, 1998). In the calculation the Hedin–Lundqvist exchange correlation potential was used with muffin-tin radii overlap of 15% (Ankudinov *et al.*, 2002*b*). A core hole was included to imitate the final state of the photon absorption process. Each type of scatterer (*i.e.* neighbor O and Ti atoms) was calculated with unique potentials (Waychunas *et al.*, 2003).

The XANES simulation was on the basis of a $\sim$8.5 Å-radius Ti–AsO_4 surface cluster model (typically $\sim$160 atoms) in which convergence had occurred. In the XANES model clusters the geometries of arsenic and the first-neighbor oxygen atoms were optimized using a density functional theory (DFT) calculation, while the TiO_2 substrate is kept frozen as the bulk structure of the anatase during the DFT calculation. The DFT-calculated small cluster model was incorporated into the large TiO_2 surface slab for XANES simulation. The XANES calculations with and without the protons on arsenate and surface hydroxyl groups showed that the effects of protons on the XANES were insignificant in this system, so the protons were neglected in the final calculation.

2.2. DFT calculation

The geometry of arsenate on TiO_2 surfaces was computed using gradient-corrected density functional theory with the Becke three-parameter non-local exchange functional (Becke, 1993) and the Lee–Yang–Parr correlation functional (Lee *et al.*, 1988) (*i.e.* B3LYP). The DFT calculation was performed using *Gaussian03* (Frisch *et al.*, 2004). Low-spin and restricted closed-shell formulae were employed. To eliminate boundary effects and reduce charge on the clusters, the dangling bonds of O atoms were saturated with H atoms (Hu & Turner, 2007; Paul *et al.*, 2006; Sherman & Randall, 2003; Zhang *et al.*, 2005). The geometry and energy were calculated using the 6-31+G(d) basis set for O and H, the 6-311+G(d) basis set for As, and the LANL2DZ relativistic effective core potential (RECP) basis set for Ti transition metal (Hu & Turner, 2007; Sun *et al.*, 2007).

For arsenate, $H_2AsO_4^-$ is the most dominant species under the experimental pH condition from 6.2 to 7.0 (Ladeira *et al.*, 2001; Sherman & Randall, 2003). Thus, the $H_2AsO_4^-$ species was used in the DFT calculation. The surfaces of anatase particles consist predominantly of (101), (100) and (001) crystal planes (Lazzeri *et al.*, 2001; Vittadini *et al.*, 1998), with the specific expression of crystal planes (*i.e.* the crystal habit) depending on the synthesis technique (Beltran *et al.*, 2001; Homann *et al.*, 2004). Our previous studies proved that the dominant surface in the TiO_2 powder used in our adsorption experiments was the (100) (He *et al.*, 2009*b*, 2011*a*), where the good agreement of calculated As–O and As–Ti distances with experimental EXAFS results indicated the reliability and agreement between the crystal planes and model cluster used in DFT calculations (see the supplementary information[1]).

In this study the dominant (101) and (100) planes of anatase were selected to construct the cluster models for XANES simulation. We used two Ti-containing surface clusters for the DFT calculation. There are two different oxygen sites in the anatase surface, O(2) and O(3), which are bonded by two and three Ti atoms, respectively (Homann *et al.*, 2004). The boundary O atoms in the model cluster were saturated with a certain amount of H atoms [12 H atoms in the Ti_2O_8 cluster of the (100) plane and 15 H atoms in the Ti_2O_9 cluster of the (101) plane] to assure that the coordination numbers of O(2) and O(3) were the same as that of the anatase surface structure. A discussion on the identification of dominant complexes has been presented in the supplementary information.

2.3. Sample preparation and XANES data collection

Arsenate stock solution was prepared from sodium arsenate ($Na_2HAsO_4{\cdot}7H_2O$, ACS, 98.0–102.0%, Alfa Aesar China) and stored at 277 K. Other reagents used in this study were analytical grade and all labware was acid-washed. Anatase TiO_2 (Beijing Chemical Regents Company, China) was used as the adsorbent. X-ray diffraction analyses showed that the TiO_2 was pure anatase. BET surface area analysis (ASAP-2010, Micromeritics) following the standard N_2-BET method indicated a specific surface area of 201.3 $m^2\ g^{-1}$ for the dry TiO_2. Because of the aggregation effect, the particle size distribution in solution, measured with a Mastersizer 2000 analyzer (Malvern, UK), ranged from 0.3 to 2.5 µm. The volume-average particle diameter was 0.95 µm. All solutions were prepared in ultrapure water (resistivity 18 MΩ) obtained with a Liyuan UPW-10N ultrapure water system.

Adsorption samples were prepared at pH 6.2 and 7.0 for X-ray absorption fine structure (XAFS) measurement. The two samples were generated by adding the same total arsenic concentration (0.80 mmol L^{-1}) to polypropylene centrifuge tubes with 1.0 g L^{-1} TiO_2, and 30 ml volume, to yield sufficient adsorption density for XAFS data collection. A constant ionic

[1] Supplementary data for this paper are available from the IUCr electronic archives (Reference: CN5033). Services for accessing these data are described at the back of the journal.

strength was maintained using 0.01 mol L^{-1} $NaNO_3$. The pH of the reaction system was constantly monitored and adjusted to the desired value (6.2 and 7.0) with addition of 0.1 mol L^{-1} NaOH or 0.1 mol L^{-1} HNO_3. The tubes were capped and shaken for 24 h at 298 K, during which the adsorption reached equilibrium. After 24 h of equilibration, the moist arsenate-laden TiO_2 solids were separated by centrifugation and mounted in 2 mm-thick sample holders. The samples were sealed between two layers of adhesive PVC tape to prevent moisture loss and stored at 277 K before XAFS measurement.

As(V) *K*-edge XAFS data were collected on beamline 4W1B at Beijing Synchrotron Radiation Facility, China. The spectra were collected under ambient conditions. The XAFS spectra of adsorption samples were collected using a Lytle ionization detector in fluorescence mode owing to the relatively low As(V) concentration (0.37 mmol g^{-1} for pH 6.2, and 0.34 mmol g^{-1} for pH 7.0). The fluorescence signal was filtered by a Ge foil and radial Soller slit assembly to reduce the elastically scattered radiation. An average of three scans was performed to achieve an adequate signal/noise ratio.

The XAFS data were processed following the standard procedures of background absorption removal and normalization using the *WinXAS3.1* software package (Ressler, 1998). A linear function fit for the pre-edge region and a second-order polynomial fit in the post-edge region were used for normalization to remove the background absorption (He *et al.*, 2011*b*; Grafe & Sparks, 2005). The experimental XANES analysis utilized the background-corrected and normalized spectra.

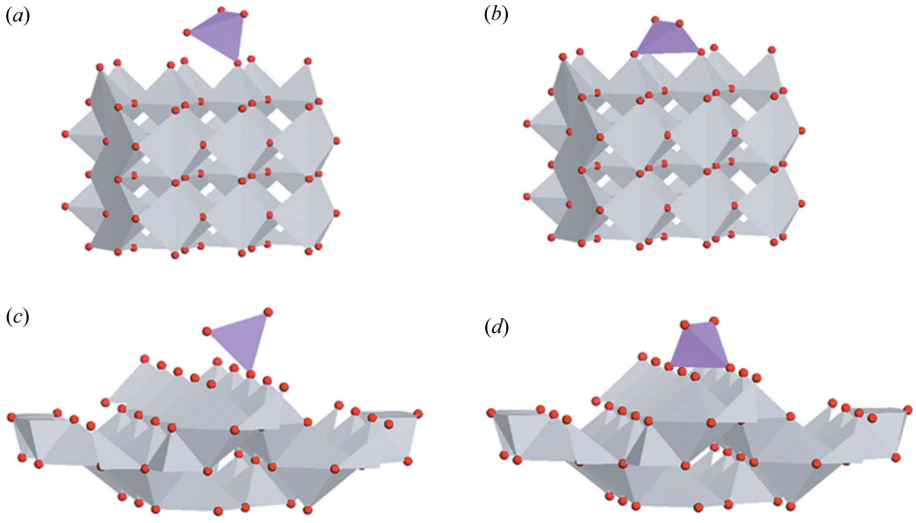

Figure 1
The cluster models used in XANES calculations. (*a*), (*b*) MM and BB complexes on the (101) plane; (*c*), (*d*) MM and BB complexes on the (100) plane. Black (purple online) and gray polyhedra denote arsenate and TiO_2 structures, respectively.

3. Results and discussion

3.1. Comparison of experimental and calculated XANES spectra

The cluster models used in the XANES calculation are shown in Fig. 1. The experimental and calculated XANES spectra are presented in Fig. 2. There was no obvious difference in experimental XANES between the two samples, suggesting a stable inner-sphere spatial population and complexation of As(V) on TiO_2 surfaces under the pH condition from 6.2 to 7.0, which was in accordance with the EXAFS-measured structural results (He *et al.*, 2009*b*).

As shown in Fig. 2(*a*), there are obvious deviations between the experimental spectra and the calculated XANES for the (101) planes, where the calculated XANES spectra showed a double-peak feature for bidentate binuclear (BB) complexes, and no absorption oscillation for monodentate mononuclear (MM) complexes in the energy area of 11883.0–11893.0 eV. The shape resonances (shapes and positions) calculated using the (101) surface cluster and those of experimental spectra did not coincide with each other in the energy area of 11910.0–

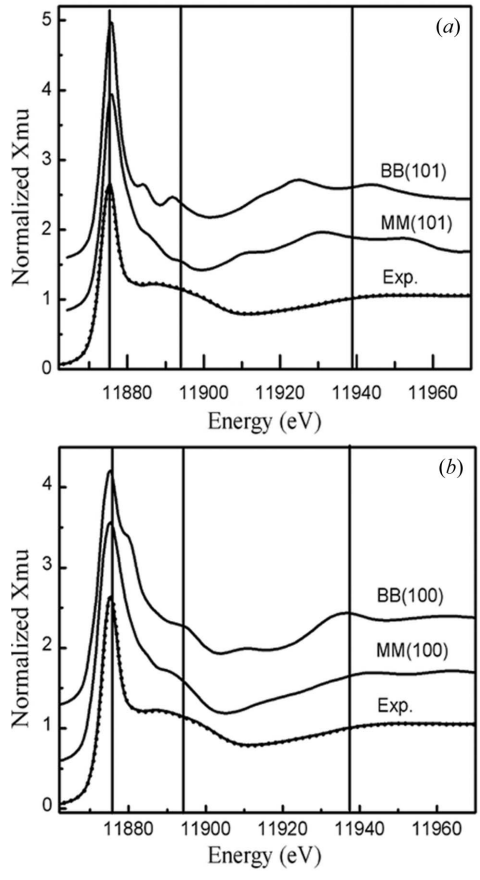

Figure 2
As(V) *K*-edge theoretical XANES spectra of MM and BB complexes and experimental XANES spectra of adsorption samples at pH 6.2 and 7.0: (*a*) the (101) plane; (*b*) the (100) plane.

11950.0 eV. Therefore, the anatase (101) surface was excluded in the theoretical analysis and calculations we describe below.

The calculated XANES spectra of MM and BB complexes using the (100) surface cluster replicated all absorption characteristics (absorption edge at 11875.0 eV, post-edge absorption oscillation at 11892.0 eV and shape resonances at 11938.0 eV) from the experimental XANES spectra (Fig. 2*b*), indicating that they were appropriate for a description of the real complexation of arsenate on TiO_2 surfaces.

Different from the low-energy XANES (from pre-edge up to ~15 eV beyond the absorption edge) that is primarily dominated by the electronic structure encompassing the target atom, high-energy XANES (from post-edge ~15 eV up to ~60 eV beyond the absorption edge) results from the single- and multiple-scattering effects from the neighbor atoms around the target atom (He *et al.*, 2009*a*; Ankudinov *et al.*, 1998). Several shape resonances that directly reproduce the distribution of the neighbor coordination atoms may be formed in the high-energy XANES area (Ankudinov *et al.*, 1998, 2002*b*). The experimentally measured two post-edge absorption characteristics (post-edge absorption oscillation at 11892.0 eV and shape resonances at 11938.0 eV) agreed with the theoretical absorption of the MM and BB surface complex (Fig. 2*b*).

Also, it can be noted that the theoretical XANES spectra of the BB complex on the (100) plane produced a shoulder at an energy position of ~5.0 eV higher than the absorption edge, which did not emerge from the experimental XANES (Fig. 2*b*). The BB complexation mode is the most commonly reported surface complex of arsenate on metal-(hydr)oxide surfaces (He *et al.*, 2009*b*; Pena *et al.*, 2006; Zhang *et al.*, 2005; Grafe & Sparks, 2005; Sherman & Randall, 2003). Detailed analysis concerning the variation in XANES features is described below.

To detect the effects of disorder on the XANES, disorder conditions of the actual system were simulated by changing the disorder parameter σ^2 in the XANES calculation (Ankudinov *et al.*, 2002*b*). As shown in Fig. 3, the shoulder above the energy of the As *K*-edge (denoted by arrows in Fig. 3) weakened when the disorder parameter σ^2 increased from 0 to 0.01, and became more less obvious as σ^2 increased to 0.02. All other absorption characteristics (absorption edge, post-edge absorption oscillation and shape resonances) weakened and broadened gradually with the increase of σ^2 from 0 to 0.02 (Fig. 3), indicating the influence of disorder on XANES features.

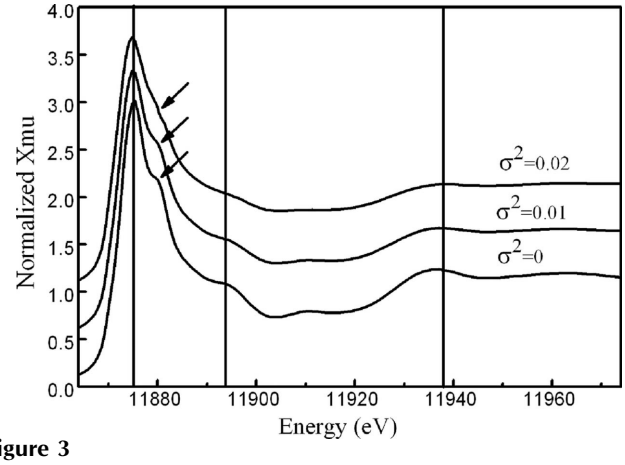

Figure 3
Calculated As(V) *K*-edge XANES spectra of the BB complex on the (100) plane with a series of Debye–Waller factors σ^2.

The disorder-containing XANES calculation reproduced the absorption characteristics of experimental XANES, where the shoulder above the absorption edge almost disappeared and the absorption characteristics of the post-edge absorption oscillation (at 11892.0 eV) and the shape resonances (at 11938.0 eV) were relatively broadening and weakening (see Fig. 2). Hence, the analyses performed here indicated that the broadening and weakening of experimental XANES characteristics were actually due to the structural disorder of the real system. The arrangement of atoms in the real system is not as ideal as that of the calculated cluster models. Therefore, the disorder-containing calculation may be more appropriate for modeling the experimental spectral features, especially for complex and low-symmetry systems. Furthermore, experimental XANES is the average spectral signal of a set of different surface complexes (He *et al.*, 2011*b*) (*e.g.* MM and BB complexes in this study). The overlapping of the scattering contributions from structurally different surface complexes also contributed to the broadening and weakening of the experimental spectral characteristics. Therefore, the XANES analysis described here suggested that the MM and BB Ti–AsO_4 complexes coexisted in one sample, a finding consistent with our EXAFS and DFT results (He *et al.*, 2011*a*; He *et al.*, 2009*b*).

3.2. Analysis of the scattering contributions from different shells to XANES

To characterize the relationship between spectral features and the local structure around the adsorbed As(V), analyses of scattering paths contributing to XANES from different coordination shells were performed using the path expansion calculation. Although the path expansion approach is unstable close to the absorption edge (Ankudinov *et al.*, 2002*b*), the spectra summed all paths reproduced well the data of the FMS calculation (Fig. 4), indicating that the path expansion approach is reliable for analyzing the spectral contributions of specific scattering paths.

The results of the path expansion calculation showed that the single/multiple scatterings of first-neighbor O atoms (<2.0 Å) contributed dominantly to the shape of the XANES, and the scattering amplitude decreased rapidly with the increase of the distance between the absorber (*i.e.* the arsenic atom) and scattering atoms (Fig. 5). The scattering amplitude of the first shell is much larger than that of the second shell (2.0–4.0 Å) over the whole XANES region, while the back-scattering intensity from the second shell is even larger than the sum of all higher-level shells (>4.0 Å). Therefore, the analyses performed here indicate that the scattering contri-

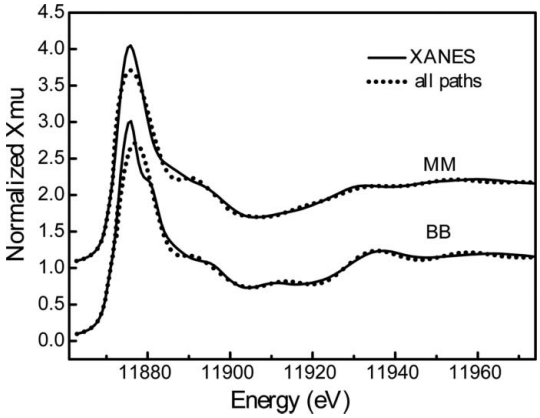

Figure 4
Theoretical As(V) *K*-edge XANES spectra of the (100) surface cluster calculated using the FMS algorithm and path expansion approach.

butions from high-level coordination shells were relatively faint because of the long photoelectron mean free path.

The scattering amplitudes of different coordination shells showed that each shell yielded not one but a set of spectral oscillations in the XANES region (Fig. 5). The single/multiple scatterings from high-level shells inherently overlapped onto the first-shell scattering amplitudes, and formed the fine structures in the XANES region. A variation in the amplitude of one oscillatory feature could be due to several structural changes affecting specific single/multiple-scattering amplitudes. Hence, an empirical assignment of one spectral feature to specific structures is generally difficult or inappropriate. The path expansion calculation of different shells showed a potential advantage to interpreting the structural origin of XANES.

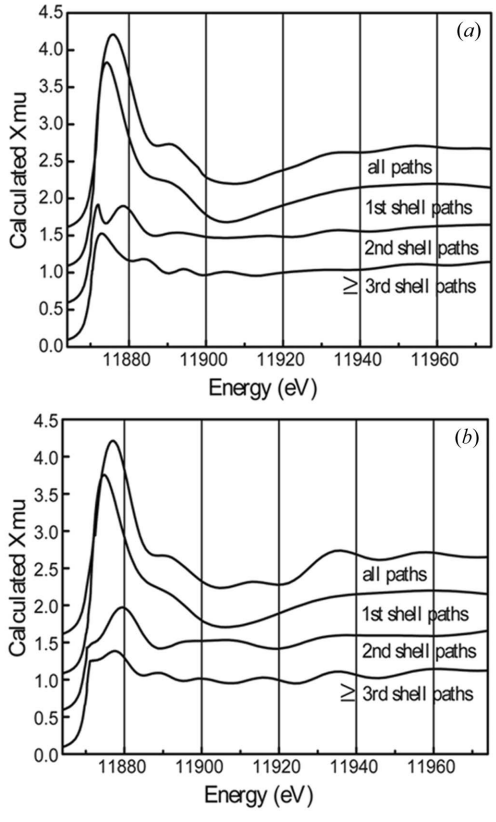

Figure 5
Simulation of the specific scattering contributions from different shells to As(V) *K*-edge XANES: (*a*) MM complex on the (100) plane; (*b*) BB complex on the (100) plane.

4. Conclusions

Ab initio calculation of XANES using self-consistent multiple-scattering methods allowed a structural analysis of the experimental spectra of arsenate adsorption on TiO_2 surfaces. The disorder-containing calculation indicated that the broadening and weakening of the experimental XANES features was due to the disorder of the adsorption system. The results of the path expansion calculation showed that the single/multiple scatterings of first-neighbor O atoms (<2.0 Å) had the highest amplitude over the whole XANES region of arsenate adsorption on TiO_2 surfaces. The scattering resonances from high-level shells inherently overlapped onto the first-shell scattering amplitudes, and formed the XANES fingerprint characteristics. All the XANES analysis indicated that direct assignments of spectral features with structural elements should be based on adequate theoretical analysis and be made with caution.

The study was supported by NNSF of China (20921063, 21007083) and the special fund from the State Key Laboratory of Environmental Aquatic Chemistry (11Y06ESPCR). We are grateful to the Beijing Synchrotron Radiation Facility (China) for providing the beam time and technical assistance in XANES simulation and analysis.

References

Ankudinov, A. L., Bouldin, C. E., Rehr, J. J., Sims, J. & Hung, H. (2002*a*). *Phys. Rev. B*, **65**, 104107.
Ankudinov, A. L., Ravel, B. & Rehr, J. J. (2002*b*). *FEFF8*, version 8.20. The FEFF Project, Department of Physics, University of Washington, USA.
Ankudinov, A. L., Ravel, B., Rehr, J. J. & Conradson, S. D. (1998). *Phys. Rev. B*, **58**, 7565–7576.
Becke, A. D. (1993). *J. Chem. Phys.* **98**, 5648–5652.
Beltran, A., Sambrano, J. R., Calatayud, M., Sensato, F. R. & Andres, J. (2001). *Surf. Sci.* **490**, 116–124.
Frisch, M. J., *et al.* (2004). *Gaussian03*, Revision C.01wis2. Gaussian Inc., Wallingford, CT, USA.
Grafe, M. & Sparks, D. L. (2005). *Geochim. Cosmochim. Acta*, **69**, 4573–4595.
He, G. Z., Pan, G. & Zhang, M. Y. (2011*a*). *J. Colloid Interface Sci.* **364**, 476–481.
He, G. Z., Pan, G., Zhang, M. Y. & Waychunas, G. A. (2011*b*). *Environ. Sci. Technol.* **45**, 1873–1879.
He, G. Z., Pan, G., Zhang, M. Y. & Wu, Z. Y. (2009*a*). *J. Phys. Chem. C*, **113**, 17076–17081.
He, G. Z., Zhang, M. Y. & Pan, G. (2009*b*). *J. Phys. Chem. C*, **113**, 21679–21686.
Homann, T., Bredow, T. & Jug, K. (2004). *Surf. Sci.* **555**, 135–144.
Hu, Z. & Turner, C. H. (2007). *J. Am. Chem. Soc.* **129**, 3863–3878.
Huang, Z. C., Chen, T. B., Lei, M., Liu, Y. R. & Hu, T. D. (2008). *Environ. Sci. Technol.* **42**, 5106–5111.
Khare, N., Martin, J. D. & Hesterberg, D. (2007). *Geochim. Cosmochim. Acta*, **71**, 4405–4415.

Ladeira, A. C. Q., Ciminelli, V. S. T., Duarte, H. A., Alves, M. C. M. & Ramos, A. Y. (2001). *Geochim. Cosmochim. Acta*, **65**, 1211–1217.
Lazzeri, M., Vittadini, A. & Selloni, A. (2001). *Phys. Rev. B*, **63**, 155409.
Lee, C. T., Yang, W. T. & Parr, R. G. (1988). *Phys. Rev. B*, **37**, 785–789.
Moniek, T., Jerome, M., Gillian, R. & John, E. (2007). *AIP Conf. Proc.* **882**, 699–701.
Morin, G., Ona-Nguema, G., Wang, Y., Menguy, N., Juillot, F., Proux, O., Guyot, F., Calas, G. & Brown, G. E. (2008). *Environ. Sci. Technol.* **42**, 2361–2366.
Nguyen, T. T., Deniau, B., Baca, M. & Millet, J. M. M. (2011). *Top. Catal.* **54**, 650–658.
Paul, K. W., Kubick, J. D. & Sparks, D. L. (2006). *Environ. Sci. Technol.* **40**, 7717–7724.
Pena, M., Meng, X., Korfiatis, G. P. & Jing, C. (2006). *Environ. Sci. Technol.* **40**, 1257–1262.
Rehr, J. J., Ankudinov, A. & Zabinsky, S. I. (1998). *Catal. Today*, **39**, 263–269.
Ressler, T. (1998). *J. Synchrotron Rad.* **5**, 118–122.
Robinet, L., Spring, M., Pagès-Camagna, S., Vantelon, D. & Trcera, N. (2011). *Anal. Chem.* **83**, 5145–5152.
Sherman, D. M. & Randall, S. R. (2003). *Geochim. Cosmochim. Acta*, **67**, 4223–4230.
Sun, Q., Altarawneh, M., Dlugogorski, B. Z., Kennedy, E. M. & Mackie, J. C. (2007). *Environ. Sci. Technol.* **41**, 5708–5715.
Vittadini, A., Selloni, A., Rotzinger, F. P. & Gratzel, M. (1998). *Phys. Rev. Lett.* **81**, 2954–2957.
Waychunas, G. A., Fuller, C. C., Davis, J. A. & Rehr, J. J. (2003). *Geochim. Cosmochim. Acta*, **67**, 1031–1043.
Yan, X. L., Chen, T. B., Liao, X. Y., Huang, Z. C., Pan, J. R., Hu, T. D., Nie, C. J. & Xie, H. (2008). *Environ. Sci. Technol.* **42**, 1479–1484.
Zabinsky, S. I., Rehr, J. J., Ankudinov, A., Albers, R. C. & Eller, M. J. (1995). *Phys. Rev. B*, **52**, 2995–3009.
Zhang, N., Blowers, P. & Farrell, J. (2005). *Environ. Sci. Technol.* **39**, 4816–4822.